

Dynamically controlled asymmetric transmission of linearly polarized waves in VO_2-integrated Dirac semimetal metamaterials

Man Xu(许曼), Xiaona Yin(殷晓娜), Jingjing Huang(黄晶晶), Meng Liu(刘蒙), Huiyun Zhang(张会云), and Yuping Zhang(张玉萍)

Citation: Chin. Phys. B, 2022, 31 (**6**): 067802. DOI: 10.1088/1674-1056/ac4bd3
Journal homepage: http://cpb.iphy.ac.cn; http://iopscience.iop.org/cpb

What follows is a list of articles you may be interested in

Optically tuned dielectric characteristics of $SrTiO_3$/Si thin film in the terahertz range

Bin Zou(邹斌), Qing-Qing Li(李晴晴), Yu-Ping Yang(杨玉平), and Hai-Zhong Guo(郭海中)
Chin. Phys. B, 2021, 30 (**10**): 107802. DOI: 10.1088/1674-1056/ac04a7

High performance terahertz anisotropic absorption in graphene-black phosphorus heterostructure

Jinming Liang(梁晋铭), Jiangtao Lei(雷江涛), Yun Wang(汪云), Yan Ding(丁燕), Yun Shen(沈云), Xiaohua Deng(邓晓华)
Chin. Phys. B, 2020, 29 (**8**): 087805. DOI: 10.1088/1674-1056/ab9cbf

Temperature dependent terahertz giant anisotropy and cycloidal spin wave modes in $BiFeO_3$ single crystal

Fan Liu(刘凡), Zuanming Jin(金钻明), Xiumei Liu(刘秀梅), Yuqing Fang(方雨青), Jiajia Guo(国家嘉), Yan Peng(彭滟), Zhenxiang Cheng(程振祥), Guohong Ma(马国宏), Yiming Zhu(朱亦鸣)
Chin. Phys. B, 2020, 29 (**7**): 077804. DOI: 10.1088/1674-1056/ab8dae

Recent progress in graphene terahertz modulators

Xieyu Chen(陈勰宇), Zhen Tian(田震), Quan Li(李泉), Shaoxian Li(李绍限), Xueqian Zhang(张学迁), Chunmei Ouyang(欧阳春梅), Jianqiang Gu(谷建强), Jiaguang Han(韩家广), Weili Zhang(张伟力)
Chin. Phys. B, 2020, 29 (**7**): 077803. DOI: 10.1088/1674-1056/ab9433

Single-shot measurement of THz pulses

Lei Yang(杨磊), Lei Hou(侯磊), Chengang Dong(董陈岗), Wei Shi(施卫)
Chin. Phys. B, 2020, 29 (**5**): 057803. DOI: 10.1088/1674-1056/ab821f

---

Dynamically controlled asymmetric transmission of linearly polarized waves in VO_2-integrated Dirac semimetal metamaterials

Man Xu(许曼)[1], Xiaona Yin(殷晓娜)[1], Jingjing Huang(黄晶晶)[1], Meng Liu(刘蒙)[1,†], Huiyun Zhang(张会云)[1,2], and Yuping Zhang(张玉萍)[1,2,‡]

[1] *College of Electronic and Information Engineering, Shandong University of Science and Technology, Qingdao* 266590, *China*
[2] *Collaborative Innovation Center of Light Manipulations and Applications, Shandong Normal University, Jinan* 250358, *China*

(Received 1 December 2021; revised manuscript received 3 January 2022; accepted manuscript online 17 January 2022)

We numerically demonstrated a novel chiral metamaterial to achieve broadband asymmetric transmission (AT) of linearly polarized electromagnetic waves in terahertz (THz) band. The proposed metamaterial unit cell exhibits no rotational symmetry with vanadium dioxide (VO_2) inclusion embedded between Dirac semimetals (DSMs) pattern. The resonant frequency of AT can be dynamically tunable by varying the Fermi energy (E_F) of the DSMs. The insulator-to-metal phase transition of VO_2 enables the amplitude of the AT to be dynamically tailored. The transmission coefficient $|T_{yx}|$ can be adjusted from 0.756 to nearly 0 by modifying the conductivity of VO_2. Meanwhile, the AT parameter intensity of linearly polarized incidence can be actively controlled from 0.55 to almost 0, leading to a switch for AT. When VO_2 is in its insulator state, the proposed device achieves broadband AT parameter greater than 0.5 from 1.21 THz to 1.80 THz with a bandwidth of 0.59 THz. When the incident wave propagates along the backward ($-z$) direction, the cross-polarized transmission $|T_{yx}|$ reaches a peak value 0.756 at 1.32 THz, whereas the value of $|T_{xy}|$ well below 0.157 in the concerned frequency. On the other hand, the co-polarized transmission $|T_{xx}|$ and $|T_{yy}|$ remained equal in the whole frequency range. This work provides a novel approach in developing broadband, tunable, as well as switchable AT electromagnetic devices.

Keywords: terahertz, chiral metamaterials, asymmetric transmission, tunable

PACS: 78.67.Pt, 42.25.Ja, 42.25.Bs **DOI:** 10.1088/1674-1056/ac4bd3

1. Introduction

Terahertz (THz) waves lie between microwave and infrared waves in the electromagnetic spectrum, and they have many unique properties,[1] including high signal-noise ratio, ultra-wideband, and strong transmission capability.[2] Natural materials have a relatively weak electromagnetic response in the terahertz band. Therefore, traditional terahertz modulators are not only inefficient, but also very thick, which is not conducive to the development of modern optical systems. Metamaterials manipulate terahertz wave at will by the arbitrary design of subwavelength microstructure array. They have been realized many novel electromagnetic effects which are not available from conventional materials, such as negative magnetic permeability,[3,4] zero refractive index,[5,6] and negative refractive index.[7] The introduction of terahertz metamaterial has promoted the development of high efficiency and integrated modulators, which have filled the "THz gap" to a large extent.[8] Asymmetric transmission (AT) devices are one of the branches of terahertz functional devices, which exhibit promising application in the development of radomes, circulators and isolators.

In 2006, Fedotov *et al.*[9] proposed AT of circularly polarized waves for the first time by using fishscale-shaped metamaterials in the optical frequency. Then in 2010, Menzel *et al.*[10] first realized AT of linearly polarized waves in three-dimensional (3D) chiral optical metamaterials. Subsequently, chiral metamaterials have been widely used to achieve AT of linearly polarized waves in the microwave[11] and terahertz regions.[12] In 2017, Fang *et al.*[13] proposed a dual-band AT device composed of five-layer metamaterial structure, which achieved strong AT effect for the linearly polarized incidence around 0.51 THz and 0.81 THz. In 2018, Stephen *et al.*[14] proposed a sandwich structure for AT of linearly polarized waves with a maximum AT parameter of 0.95 in the microwave band. However, once these devices have been fabricated, their working frequency and amplitude cannot be controlled in real time, which seriously limits their practical application.

In order to overcome the above bottlenecks and obtain THz devices with dynamically controlled performance, materials with adjustable electromagnetic properties are combined into metamaterial structures, such as graphene,[15–19] Dirac semimetals (DSMs),[20] and vanadium dioxide (VO_2).[21–24] These tunable metamaterial structures

†Corresponding author. E-mail: liumeng0231@tju.edu.cn
‡Corresponding author. E-mail: sdust_thz@163.com
© 2022 Chinese Physical Society and IOP Publishing Ltd

are conducive to the development of novel terahertz devices, such as modulators,[25–28] filters,[25–28] and sensors.[25–27] Zhao *et al.*[15] proposed a three-layer metal–graphene–metal metasurface to achieve the tunability of linear AT by varying the Fermi energy of the graphene. However, graphene exhibits an instable property and interact light weakly since it is composed of single layer atom,[29] which limits its development of high efficiency AT devices. DSMs are considered to be analogues of three-dimensional graphene. In comparison, it has higher electron mobility[30,31] and interacts with incident waves strongly.[32] Furthermore, the Fermi energy of DSMs can be by alkaline surface doping.[33,34] These excellent properties make DSMs a suitable candidate material for the construction of actively controlled metamaterial absorbers,[35–38] electromagnetic induced transparency[39–43] devices, polarization conversion devices.[44,45] Dai *et al.*[20] designed AT devices for linearly polarized waves based on DSMs. The proposed device achieves a maximum AT parameter of 0.38 at 1.56 THz, and the resonant frequency and amplitude were dynamically tunable by changing the DSMs Fermi energy. However, the tunability of the resonant frequency was accompanied by a reduction in the AT intensity as the decrease of the DSMs Fermi level. It is well-known that VO_2 exhibits a phase transition from an insulating dielectric state to a metallic state[42] via electrical, thermal, and optical stimuli.[46–48] During the transition progress, VO_2 undergoes a drastic change in conductivity exceeding four orders of magnitude around the critical temperature 68°. Recently, Liu *et al.*[21] carried out a systematic research on temperature-controlled two-dimensional (2D) chirality and 3D chirality in the terahertz regime, including the dynamically controlled linearly polarized AT,[22] switchable chiral mirrors,[23] and actively controlled negative refractive index.[24] However, all AT of linearly polarized devices were designed cannot simultaneously realize these two functionalities. Firstly, the resonant frequency of the AT is dynamically tunable while maintaining the amplitude of AT. Then, the amplitude can be dynamically tuned independently leading to a switch for AT.

In this work, we proposed a theoretical AT device based on VO_2 and DSMs in the terahertz region. At the room temperature, VO_2 is in its insulating state, tunable broadband AT of linearly polarized terahertz waves has been achieved. The resonant frequency can be dynamically tuned by modifying the Fermi level of DSFs while maintaining the amplitude of AT. Increasing the operation temperature across 68 °C, VO_2 transmit from insulating state to metallic state, the AT amplitude of linearly polarized waves decrease significantly, while the resonant frequency remains the same almost be almost unchanged. This work can be used to inspire the fabrication of tunable AT devices in the terahertz range, as well as the similar modulator operating in other frequency.

2. Design and theoretical analysis

Figure 1 illustrates the schematic of a unit cell of the proposed chiral metasurface, which consists of three layers. The top layer composed of DSMs and VO_2 microstructures, which a 6-shaped structure with a thickness of 0.7 μm. The 6-shaped patterns on the front and back surfaces of the dielectric layer are structurely identical and the bottom pattern is a mirror image of the top layer rotated by 90°. The polyimide layers have been treated as a lossy material with dielectric constant set to $\varepsilon_p = 3 + 0.09\mathrm{i}$,[49] and its thickness is 21 μm. The width of DSMs bars is $w = 3$ μm, and the gap between DSMs bars is $g = 3$ μm. The period of the unit is $P = 20$ μm. When VO_2 in its insulating state, this chiral metasurface can achieve AT effect shown in Fig. 1(a). VO_2 transmit from insulating state to metallic state, AT can be turned off shown in Fig. 1(b). The electromagnetic simulation software CST Microwave Studio is used to simulate the chiral metasurface. In simulations, the unit cell boundary conditions are employed along the x and y directions, and the open boundary condition is applied along the z direction.

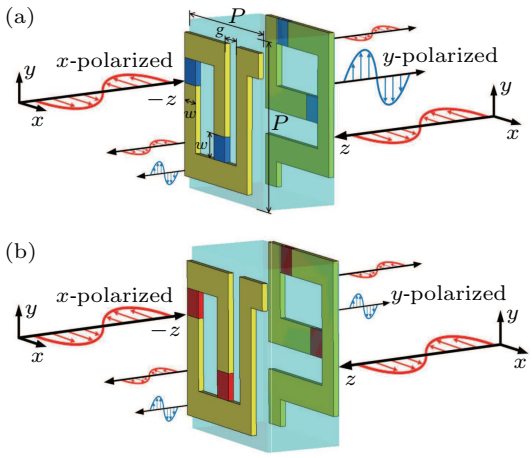


Fig. 1. Transmission schematic diagrams of hybrid DSMs-VO_2 metasurface. (a) When VO_2 is in the insulating state (10 S/m), the device in form of AT is turned on (shown in blue). (b) When VO_2 serves as a dielectric (10^5 S/m), the device in form of AT is turned off (shown in red).

In the range of long wave limit $q \ll K_F$, the longitudinal dynamic conductivity formula of DSMs can be obtained by Kubo formula in random-phase approximation theory. The conductivity of DSMs can be calculated by the formula $\delta(w) = \delta_{\mathrm{intra}}(w) + \delta_{\mathrm{inter}}(w)$, where $\delta_{\mathrm{intra}}(w)$ and $\delta_{\mathrm{inter}}(w)$ are the intraband and interband conductivity respectively. The interband and intraband conductivity of the DSMs can be defined as[50]

$$\delta_{\mathrm{intra}}(w) = \frac{\mathrm{i}e^2}{\hbar}\frac{gk_F}{6\pi^2\Omega}\left(1 + \frac{\pi^2}{3}\left(\frac{T}{E_F}\right)^2\right), \tag{1}$$

$$\delta_{\text{inter}}(w) = \frac{\mathrm{i}e^2 gw}{3\pi^2\hbar v_{\text{F}}}\left[-\frac{\pi\mathrm{i}}{2}\frac{G(\hbar w/2)}{4} + \int_0^{\infty}\left(\frac{G(E)-G(\hbar w/2)}{\hbar^2 w^2 - 4E^2}\right)E\,\mathrm{d}E\right]. \quad (2)$$

In the formula, $k_{\text{F}} = E_{\text{F}}/(\hbar v_{\text{F}})$ is the Fermi momentum, $\hbar$ is the Planck constant, E_{F} is the Fermi level, $v_{\text{F}} \approx 10^6$ m/s is the Fermi speed, $\Omega = \hbar w/E_{\text{F}} + \mathrm{i}h\tau^{-1}/E_{\text{F}}$, where $\tau = \mu E_{\text{F}}/ev_{\text{F}}^2$ and μ is carrier mobility,[51] w is the frequency. $G(E) = n(-E) - n(E) = \sinh(E/T)/\cosh(E_{\text{F}}/T) + \cosh(E/T)$, where $E = hw/2$ and $n(E)$ is the Fermi distribution function. Here, the dielectric constant of DSMs is represented by a two-band model

$$\varepsilon = \varepsilon_{\text{b}} + \mathrm{i}\frac{\sigma}{w\varepsilon_0}, \quad (3)$$

where ε_0 is the permittivity of a vacuum and the effective background dielectric is $\varepsilon_{\text{b}} = 1$ for $g = 40$ (AlCuFe quasicrystals[50]).

VO_2 undergo a phase change under thermal control and during the simulation the dielectric constant is described by the Drude model[52]

$$\varepsilon(w) = \varepsilon_{\infty} - \frac{w_{\text{p}}^2(\sigma)}{w^2 + \mathrm{i}\gamma w}, \quad (4)$$

where the permittivity at an infinite frequency is $\varepsilon_{\infty} = 12$ and the damping frequency is $\gamma = 5.75 \times 10^{13}$ rad/s.[53] The plasma frequency is expressed as $w_{\text{p}}(\sigma) = (\sigma/\sigma_0)w_{\text{p}}^2(\sigma_0)$, where $\sigma_0 = 3 \times 10^5$ S/m and $w_{\text{p}}^2(\sigma) = 1.4 \times 10^{15}$ rad/s. In the simulation, the conductivity of VO_2 is increased from 10 S/m to 10^5 S/m to represent the transition from an insulating to the metallic state.[42] Specifically, it is assumed that VO_2 is in a metallic (insulating) state with a conductivity of 10^5 S/m (10 S/m).

The complex amplitudes of incident and transmitted waves can be linked with Jones matrix T to better understand the AT phenomenon,[10] which can be expressed as

$$\begin{pmatrix} T_x \\ T_y \end{pmatrix} = \begin{pmatrix} T_{xx} & T_{xy} \\ T_{yx} & T_{yy} \end{pmatrix}\begin{pmatrix} I_x \\ I_y \end{pmatrix} = T_{\text{lin}}^{f}\begin{pmatrix} I_x \\ I_y \end{pmatrix}, \quad (5)$$

where T_{xx}, T_{yy} and T_{xy}, T_{yx} represent the co-polarization and the cross-polarization transmission coefficients, respectively. I_x, I_y and T_x,T_y represent the complex amplitudes of the incident and transmitted waves. lin and f indicate that the linearly polarized waves propagate in the forward ($+z$) direction.

The AT response is usually characterized by the difference of transmission between forward and backward propagation for linearly polarized waves.[49] The AT parameters of linearly waves can be expressed as[54] (the superscript "b" means along the backward direction):

$$\Delta_{\text{lin}}^{x} = |T_{xx}^{\text{f}}|^2 + |T_{yx}^{\text{f}}|^2 - |T_{xx}^{\text{b}}|^2 - |T_{yx}^{\text{b}}|^2 = -\Delta_{\text{lin}}^{y}. \quad (6)$$

Since the 6-shaped patterns on the front and back surfaces of the dielectric layer have the characteristic of chirality, the co-polarized transmission coefficients of linearly polarized waves are always equal. The formula can be further simplified as

$$\Delta_{\text{lin}}^{x} = |T_{yx}|^2|T_{xy}|^2 = -_{\text{lin}}^{y}. \quad (7)$$

It can be seen from the Eq. (7) that the AT of linearly polarized waves result from the cross-polarized transmission coefficients.

Stokes parameters are used to verify the polarization conversion performance of linearly polarized waves, which can be expressed as:[44]

$$I = |T_{xx}|^2 + |T_{yx}|^2, \quad (8)$$

$$Q = |T_{xx}|^2| - T_{yx}|^2, \quad (9)$$

$$U = 2|T_{yx}||T_{xx}|\cos\Delta\varphi, \quad (10)$$

$$V = 2|T_{yx}||T_{xx}|\sin\Delta\varphi, \quad (11)$$

where $\Delta\varphi$ is the phase difference between the cross- and co-polarized components. In addition, the polarization rotation angle θ and the ellipticity η[2] can be expressed respectively by

$$\theta = \frac{1}{2}\tan^{-1}\left(\frac{U}{Q}\right), \quad (12)$$

$$\eta = \frac{1}{2}\sin^{-1}\left(\frac{V}{I}\right). \quad (13)$$

3. Results and discussion

The spectra response of the proposed device has been demonstrated for the case where VO_2 is in the insulating dielectric state with conductivity of 10 S/m, and the Fermi energy level of the DSMs is 0.15 eV. Figures 2(a) and 2(b) show the four elements of the transmission matrix for a linearly polarized wave propagating along the backward ($-z$) and forward ($+z$) directions. For the y-polarized waves propagating in the backward direction and the x-polarized waves propagating in the forward direction, the AT device allows waves to transmit through themselves with a perfect diode effect. As shown in Fig. 2(a), the co-polarization transmission coefficients (T_{xx}, T_{yy}) are always equal over the entire frequency range, while the cross-polarization transmission coefficients (T_{xy}, T_{yx}) are significantly different. The value of $|T_{yx}|$ is higher than 0.7 and $|T_{xy}|$ is lower than 0.16 in the range of 1.184 THz–1.8336 THz. Compared with Figs. 2(a) and 2(b), when the propagation direction is switched, the co-polarized transmission coefficients remains unchanged, while cross-polarized transmission coefficients will exchange. It can be observed from Figs. 2(c) and 2(d), when the x-linearly polarized waves propagating along

the backward direction, the polarization azimuth is 88.1° and −68.8° at 1.184 THz and 1.8336 THz. Therefore, these phenomena are identical to the conditions required for the AT effect that cause AT of linearly polarized waves.

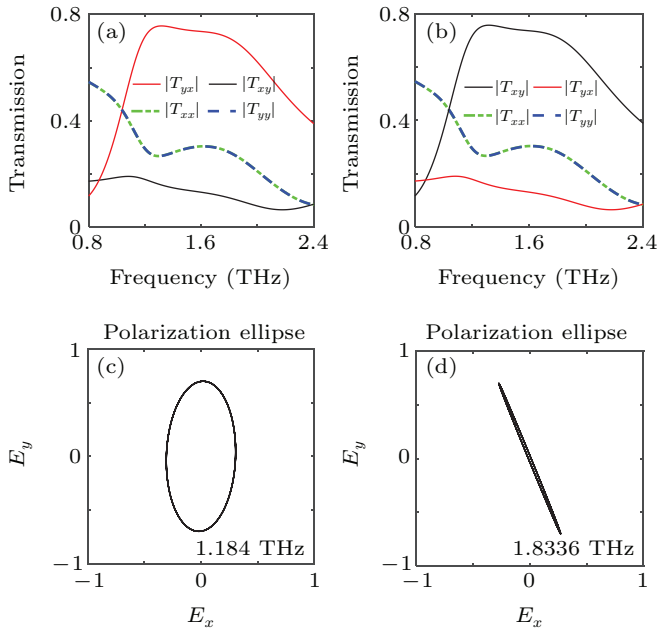


Fig. 2. Transmission coefficients of linearly polarized waves propagating along the (a) backward (−z) and (b) forward (+z) directions. Polarization ellipse of the transmitted waves at (c) 1.184 THz and (d) 1.8336 THz with an incident x-polarized waves propagating along the backward (−z) direction.

According to Eqs. (6) and (7), we calculate the AT parameters for a linearly incident wave along the backward direction shown in Fig. 3(a). When increasing the frequency, the value of parameter for a linearly polarized wave experiences a rapid increase and reaches the maximum of 0.55 at frequency of 1.30 THz. The AT parameter greater than 0.5 in the frequency range 1.21 THz–1.80 THz and a bandwidth of 0.59 THz. $\Delta_{\rm lin}^{(x)}$ and $\Delta_{\rm lin}^{(y)}$ curves have approximately opposite trends and the absolute values are always the same. The device achieves an AT response for linearly polarized waves in the broadband range.

The AT performance can be described more intuitively by introducing the polarization conversion ratio (PCR) and the total transmission intensity (T) of the x- and y-linearly polarized waves. The equations $\mathrm{PCR}_x = |T_{yx}|^2/(|T_{xx}|^2 + |T_{yx}|^2)$ and $\mathrm{PCR}_y = |T_{xy}|^2/(|T_{yy}|^2 + |T_{xy}|^2)$ are used to illustrate the performance of the x- and y-linear PCR_x and PCR_y shown in Fig. 3(b). PCR_x is greater than 0.8 in the range of 1.15 THz–2.4 THz, indicating that most of the x-polarized waves are converted to$y$-polarized waves. The equations $|T_x|^2 = |T_{xx}|^2 + |T_{yx}|^2$ and $|T_y|^2 = |T_{yy}|^2 + |T_{xy}|^2$ represent the total transmittance of x- and y-polarized waves. Figure 3(c) shows the total transmission intensity of linearly polarized waves propagating from the forward and backward directions respectively. Total transmission intensity $T_x^{\rm b}$ of x-polarized waves incident along backward direction shows one peak of 0.64 at 1.33 THz, while total transmission intensity $T_y^{\rm b}$ of y-polarized waves is relatively low.

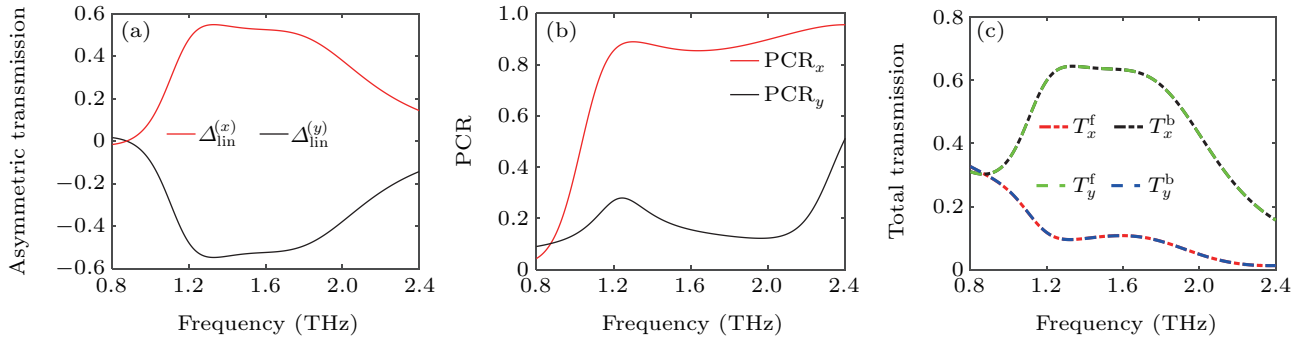


Fig. 3. (a) AT parameters for linearly polarized waves propagating along the backward direction. (b) PCR for x- and y-polarized waves propagating in the backward direction. (d) Total transmission for linearly polarized waves propagating in the backward and forward directions.

According to Eqs. (12) and (13), we calculate the polarization rotation angle θ and ellipticity η of linearly polarized waves propagating in the backward direction shown in Figs. 4(a) and 4(b). As can be seen from Fig. 4(a), the polarization azimuth of the x-polarized waves at 1.2 THz is close to 90°, achieving a perfect x–y polarization conversion. However, the absolute value of y-polarized waves in the whole frequency range is less than 25°, so it can hardly be converted into x-polarized waves when passing through the device. The incident linearly polarized waves change into linearly or elliptically polarized waves after passing through the chiral structure as shown in Fig. 4(b). The $\eta$of x-polarized and y-polarized is 0 at the frequency 1.79 THz, which indicate that the transmitted wave is still linearly polarized. In the frequency range of less than 1.79 THz, the η of x-polarized wave is less than 0, thus the transmitted wave becomes right-handed elliptical polarized one. When the frequency is greater than 1.79 THz, η is always more than 0, and the transmitted wave is left-handed circular polarization.

Figure 5 shows the four transmission matrices at different Fermi levels when the linearly polarized waves propagating in the backward direction. When the Fermi level of DSMs is

modified from 0.05 eV to 0.15 eV, the amplitude of transmission coefficients are basically unchanged and the resonant frequency are blue shifted. Therefore, changing the Fermi level of the DSMs can achieve dynamic tunability of resonant frequency, thus increasing the applications of devices.

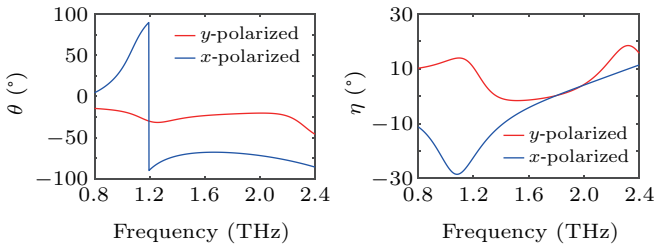


Fig. 4. Polarization azimuth (a) and ellipticity angle (b) for linearly polarized waves propagating along the backward direction.

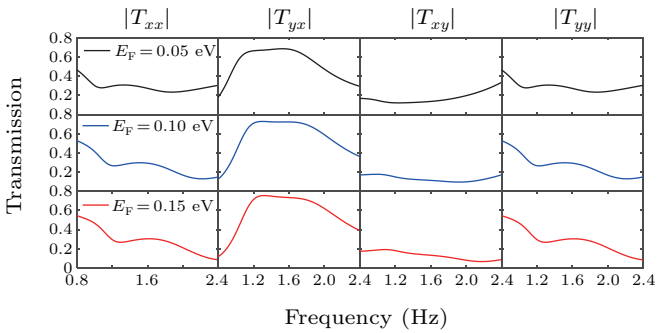


Fig. 5. The transmission coefficients for four transmission matrices propagating in the backward direction at different Fermi energy of DSMs.

By analyzing the electric field of linearly polarized waves propagating in the backward direction, the AT effect can be more clearly understood. Figure 6(a) shows that the direction of the electric field changes from horizontal to vertical as the x-polarized waves are incident, which indicates that the x–y polarization transition is achieved at 1.30 THz. In contrast, the direction of the electric field of the output wave is still vertical when the y-polarized waves propagate, as shown in Fig. 6(b).

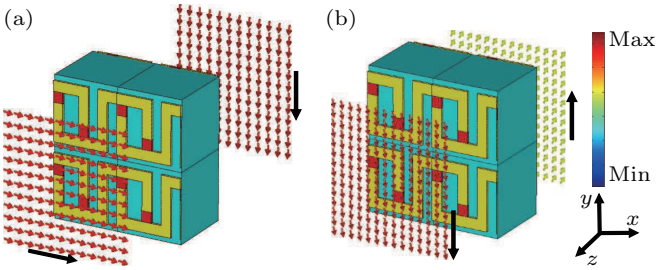


Fig. 6. Calculated electric field distributions at 1.30 THz for x-polarized waves (a) and y-polarized waves (b) propagating in the backward direction.

Figure 7(a) shows that the backward propagating x-polarized incidence takes AT parameters with different incident angles. The angle of incidence has essentially no effect on $\Delta_{\text{lin}}^{(x)}$ when the angle of incidence is less than 40°. When the incident angle is greater than 40°, the AT intensity decreases to 0 with the increase of incident angle α. It can be seen from Fig. 7(b) that the absolute value of $\Delta_{\text{lin}}^{(x)}$ of AT decreases to 0 and then increases with the increase of the polarization angle θ.

The intensity of the four transmission matrices can be tailored by modifying the conductivity of VO_2 as shown in Fig. 8(a). When the x- and y-linearly polarized waves propagate in the backward direction, the cross-polarized transmission coefficients $|T_{yx}|$ and $|T_{xy}|$ decrease continuously as the metallic properties of VO_2 increase. However, the co-polarized transmission coefficients $|T_{xx}|$ and $|T_{yy}|$ increase continuously. Therefore, the curves in Fig. 8(a) will form the phenomenon in Figs. 8(b) and 8(c). It can be seen from Fig. 8(b) that AT parameter Δ_{lin}^{x} continuously decreases by increasing the conductivity of the VO_2. The phenomenon of AT basically disappears when the conductivity is 10^5 S/m. With the conductivity of VO_2 increase, the rising conductivity leads to a continuous decrease in transmission, as shown in Fig. 8(c). Thus, AT occurs when VO_2 is in the insulator state and it can be turned off by increasing its conductivity.

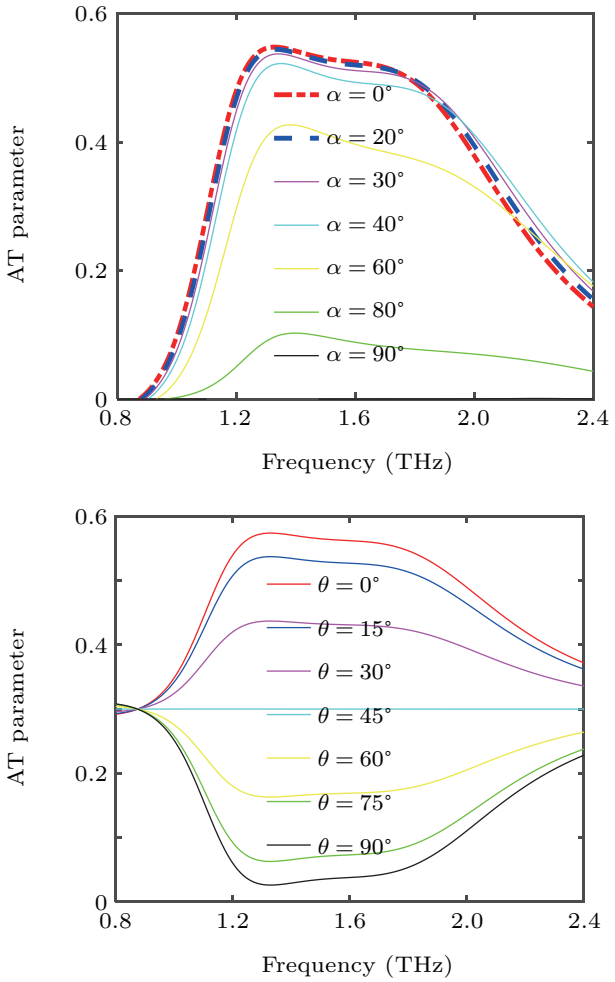


Fig. 7. AT parameters as a function of (a) incident angle α and (b) polarization angle θ for x-linearly polarized waves propagating in the backward direction.

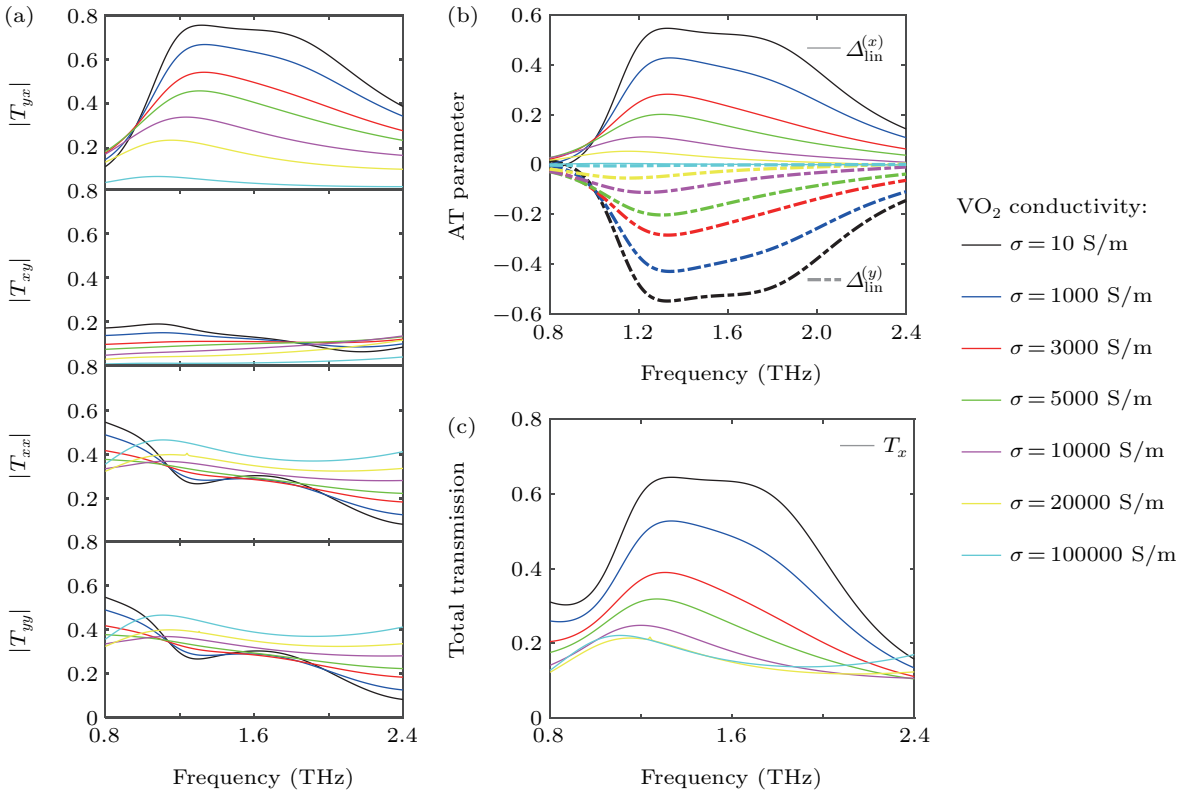


Fig. 8. (a) Four transmission matrices, (b) AT parameters and (c) total transmission intensity for linearly polarized waves propagating in the backward direction under different conductivity of VO_2 ($E_F = 0.15$ eV).

4. Conclusion

In this work, we have realized a dynamically controlled broadband AT device for linearly polarized terahertz waves based on DSMs and VO_2 materials. When the VO_2 in its insulating state (10 S/m), the bandwidth of AT parameter greater than 0.5 is 0.59 THz in the frequency range of 1.21 THz–1.80 THz. When the VO_2 in its metallic state (10^5 S/m), the AT parameter is almost 0 in the entire frequency range of 0.8 THz–2.4 THz. Therefore, the amplitude of AT can be dynamically tailored by modifying the conductivity of VO_2. The resonant frequency of AT exhibits blue shift with the Fermi level of DSMs increases from 0.05 eV to 0.15 eV while maintaining the amplitude of AT. The method of adjusting resonant frequency and amplitude independently increases the practicability of devices, which is conducive to the development of AT devices.

Acknowledgments

Project supported by the National Natural Science Foundation of China (Grant Nos. 61875106, 62105187, and 61775123), the Natural Science Foundation of Shandong Province, China (Grant No. ZR2021QF010), the Shandong Social Science Planning Project, China (Grant No. 21CZXJ08), and the National Key Research and Development Program of China (Grant No. 2017YFA0701000).

References

[1] Tonouchi M 2007 *Nat. Photon.* **1** 97
[2] Zhang H Y, Yang C H, Liu M and Zhang Y P 2021 *Results Phys.* **25** 104242
[3] Ozbay E, Guven K and Aydin K 2007 *J. Opt. A-Pure Appl. Op.* **9** S301
[4] Wang Anna, Tuniz Alessandro, Hunt Peter G, Pogson Elise M, Lewis Roger A, Bendavid Avi, Fleming Simon C, Kuhlmey Boris T and Large C J 2011 *Opt. Mater. Express* **1** 115
[5] Liu Y, Guo X, Gu S and Zhao X 2013 *Int. J. Antenn. Propag.* **2013** 1098
[6] Koutserimpas T T and Fleury R 2018 *J. Appl. Phys.* **123** 091709
[7] Soukoulis C M, Linden S and Wegener M 2007 *Science* **315** 47
[8] Williams G P 2006 *Rep. Prog. Phys.* **69** 301
[9] Fedotov V A, Mladyonov P L, Prosvirnin S L, Rogacheva A V, Chen Y and Zheludev N I 2006 *Phys. Rev. Lett.* **97** 167401
[10] Menzel C, Helgert C, Rockstuhl C, Kley E -B, Tünnermann A, Pertsch T and Lederer F 2010 *Phys. Rev. Lett.* **104** 253902
[11] Cheng Y Z, Nie Y, Wang X and Gong R Z 2013 *Appl. Phys. A* **111** 209
[12] Cheng Y Z, Gong R Z and Wu L 2017 *Plasmonics* **12** 1113
[13] Fang S Y, Kang L, Ma H F, Lv W J, Li Y X, Zhu Z, Guan C Y, Shi J H and Cui T J 2017 *J. Appl. Phys.* **121** 033103
[14] Stephen L, Yogesh N and Subramanian V 2018 *J. Appl. Phys.* **123** 033103
[15] Zhao J X, Song J L, Xu T Y, Yang T X and Zhou J H 2019 *Opt. Express* **27** 9773
[16] Li Z C, Liu W W, Cheng H, Chen S and Tian J G 2016 *Opt. Lett.* **41** 3142
[17] Huang Y Y, Yao Z H, Hu F R, Liu C J, Yu L L, Jin Y P and Xu X L 2017 *Carbon* **119** 305
[18] Zhao J Y, Zhang J F, Zhu Z H, Yuan X D and Qin S Q 2016 *J. Opt.* **18** 095001
[19] Zhang Y P, Li Tong Tong, Lv H H, Huang X Y, Zhang X, Xu S L and Zhang H Y 2015 *Chin. Phys. Lett.* **32** 068101
[20] Dai L L, Zhang H Y, O'Hara J F and Zhang Y P 2019 *Opt. Express* **27** 35784
[21] Li Tong, Hu F Q, Qian Y X, Xiao J, Zhang L H, Zhang W T and Han J G 2019 *Chin. Phys. B* **29** 024203
[22] Liu M, Xu Q, Chen X, Plum E, Li H, Zhang X Q, Zhang C H, Zhou C W, Han J G and Zhang W L 2019 *Sci. Rep-UK.* **9** 4097

[23] Liu M, Plum E, Li H, Duan S Y, Li S X, Xu Quan, Zhang X Q, Zhang C H, Zou C W, Jin B B, Han J G and Zhang W L 2020 *Adv. Opt. Mater.* **8** 2000247

[24] Liu M, Plum Eric, Li H, Li S X, Xu Q, Zhang X Q, Zhang C H, Zou C W, Jin B B, Han J G and Zhang W L 2021 *Adv. Funct. Mater.* **31** 2010249

[25] He X Y, Liu F, Lin F T and Shi W Z 2021 *J. Phys. D* **54** 235103

[26] Leng J, Peng J, Jin A, Cao D, Liu D J, He X Y, Lin F T and Liu F 2022 *Opt. Laser Technol.* **146** 107570

[27] Peng J, He X Y, Shi C Y Y, Leng J, Lin F T, Liu F, Zhang H and Shi W Z 2020 *Physica E* **124** 114309

[28] He X Y, Lin F T, Liu F and Shi W Z 2022 *Opt. Mater. Express* **12** 73

[29] Xu Z H, Wu D, Liu Y M, Liu C, Yu Z Y, Yu L and Ye H 2018 *Nanoscale Res. Lett.* **13** 143

[30] He L P, Hong X C, Dong J K, Pan J, Zhang Z, Zhang J and Li S Y 2014 *Phys. Rev. Lett.* **113** 246402

[31] Chen Z, Wu M, Liu Y Q, Gao W S, Han Y Y, Zhou J Z, Ning W and Tian M L 2021 *Chin. Phys. Lett.* **38** 047201

[32] Zdanowicz W and Zdanowicz L 1975 *Annu. Rev. Mater. Res.* **5** 301

[33] Liu Z K, Jiang J, Zhou B, Wang Z J, Zhang Y, Weng H M, Prabhakaran D, Mo S-K, Peng H, Dudin P, Kim T, Hoesch M, Fang Z, Dai X, Shen Z X, Feng D L, Hussain Z and Chen Y L 2014 *Nat. Mater.* **13** 677

[34] Liu Z K, Zhou B, Zhang Y, Wang Z J, Weng H M, Prabhakaran D, Mo S K, Shen Z X, Fang Z, Dai X, Hussain Z and Chen Y L 2014 *Science* **343** 864

[35] Li Z Y, Yi Y T, Xu D Y, Yang H, Yi Z, Chen X F, Yi Y G, Zhang J G and Wu P H 2021 *Chin. Phys. B* **30** 098102

[36] Meng H Y, Shang X J, Xue X X, Tang K Z, Xia S X, Zhai X, Liu Z R, Jiang J H, Li H J and Wang L L 2019 *Opt. Express* **27** 31062

[37] Jiang Y, Wang X G, Wang J and Wang J 2018 *IEEE Photon. J.* **10** 4600607

[38] Xiong H, Shen Q and Ji Q 2020 *Appl. Opt.* **59** 4970

[39] Zhao J X, Song J L, Zhou Y, Zhao R L and Zhou J H 2019 *Opt. Mater. Express* **9** 3325

[40] Fan C Z, Ren P W, Jia Y L, Zhu S M and Wang J Q 2021 *Chin. Phys. B* **30** 096103

[41] Shen S M, Liu Y L, Liu W Q, Tan Q L, Xiong J J and Zhang W D 2018 *Mater. Res. Express* **5** 125804

[42] Cao M Y, Wang T L, Li L, Zhang H Y and Zhang Y P 2020 *J. Opt. Soc. Am. A* **37** 1340

[43] Chen H, Zhang H Y, Liu M D, Zhao Y K, Guo X H and Zhang Y P 2017 *Opt. Mater. Express* **7** 3397

[44] Dai L L, Zhang Y P, Guo X H, Zhao Y K, Liu S D and Zhang H Y 2018 *Opt. Mater. Express* **8** 3238

[45] Dai L L, Zhang Y P, Zhang H Y and O'Hara J F 2019 *Appl. Phys. Express* **12** 075003

[46] Jepsen P U, Fischer B M, Thoman A, Helm H, Suh J Y, Lopez R and Haglund R F 2006 *Phys. Rev. B* **74** 205103

[47] Wen Q Y, Zhang H W, Yang Q H, Xie Y S, Chen K and Liu Y L 2010 *Appl. Phys. Lett.* **97** 021111

[48] Zhang C, Zhou G, Wu J, Tang Y, Wen Q, Li S, Han J, Jin B, Chen J and Wu P 2019 *Phys. Rev. Appl.* **11** 054016

[49] Lv T T, Chen X Y, Dong G H, Liu M, Liu D M, Ouyang C M, Zhu Z, Li Y X, Guan C Y, Han J H, Zhang W L, Zhang S and Shi J H 2020 *Nanophotonics* **9** 3235

[50] Kotov O V and Lozovik Yu E 2016 *Phys. Rev. B* **93** 235417

[51] Liu G D, Zhai X, Meng H Y, Liu Q, Huang Y, Zhao C J and Wang L L 2018 *Opt. Express* **26** 11471

[52] Chen L L and Song Z Y 2020 *Opt. Express* **28** 6565

[53] Song Z Y, Deng Y D, Zhou Y G and Liu Z Y 2019 *Opt. Express* **27** 5792

[54] C Menzel, C Rockstuhl and F Lederer 2010 *Phys. Rev. A* **82** 053811